Prospects for an independent measurement of the $\ell = 1, 2, 3$ CMB anisotropy multipoles using the anisotropic Sunyaev-Zel'dovich effect

D. I. Novikov,[1] T. I. Larchenkova,[1] A. O. Mihalchenko,[1] A. M. Osipova,[1,2] K. O. Parfenov,[1] and S. V. Pilipenko[1,2]

[1]*Astro-Space Center of P.N. Lebedev Physical Institute, Profsoyusnaya 84/32, Moscow 117997, Russia*
[2]*HSE University, 101000 Moscow, Russia*

(Received 30 June 2025; accepted 24 July 2026; published 14 September 2026)

We investigate the prospects for observing a specific spectral distortion of the cosmic microwave background, which occurs due to the anisotropy of the radiation when it is scattered by hot plasma of galaxy clusters. Detection of this anisotropic Sunyaev-Zel'dovich effect would enable an independent measurement of the CMB anisotropy multipoles with $\ell = 1, 2, 3$, allow the Sachs-Wolfe and integrated Sachs-Wolfe (Rees-Sciama) effects to be separated, and partially solve the cosmic variance problem for low multipoles. We applied the Least Response Method for component separation in the data processing and estimated the required sensitivity of the experiment for such observations. We test our approach on a simulated signal that is contaminated by various foregrounds with poorly defined spectral shapes, along with distortions of the relic blackbody spectrum caused by the Sunyaev-Zel'dovich effect and its relativistic corrections.

DOI: 10.1103/vd13-8dbj

I. INTRODUCTION

Measurements of the cosmic microwave background (CMB) temperature anisotropy by WMAP [1] and Planck [2,3] show alignment of the quadrupole and octupole [4–6] and a lack of power of multipoles with low ℓ in the observed angular spectrum C_ℓ [2,7–9]. In addition, according to the studies [10–15], there are other large-scale anomalies in the temperature maps of the relic radiation. These observations are difficult to reconcile with the predictions of Gaussian statistics and the standard inflationary model. Such anomalies may be due to incomplete removal of foreground components, particularly those from the Milky Way. The intrinsic cosmological dipole is completely masked by the dipole induced by our motion with respect to the CMB rest frame. Besides, the observed anisotropy map represents only one realization of a random process, which inevitably leads to the "cosmic variance" problem for low multipoles.

This motivates the search for an independent source of information on the low-order anisotropy multipoles beyond the directly observed CMB sky. This source of information should not be so sensitive to the specific spatial distribution of foregrounds in our vicinity, should not depend on our motion relative to the CMB rest frame, and should help us at least partially get around the cosmic variance problem.

One possible way to obtain such alternative information on low multipoles is to observe the anisotropic Sunyaev-Zel'dovich effect (aSZ) described in Refs. [16,17]. The impact of radiation anisotropy on the scattered frequency spectrum is also investigated in Ref. [18]. This effect is a correction to the well-known thermal Sunyaev-Zel'dovich effect (tSZ) [19,20] due to the anisotropy of radiation scattered by hot electron plasma of galaxy clusters.

According to Ref. [21], the first correction to the Thomson scattering cross section is proportional to the electron temperature $\Theta_e = k_B T_e / m_e c^2$ and effectively depends on the scattering angle. Using this fact, it is shown in Refs. [16,17] that in the linear approximation in Θ_e the dipole, quadrupole, and octupole components of the anisotropic radiation incident on the cluster create a distinctive spectral distortion of the scattered radiation. The amplitude of this distortion is proportional to $\sim\Theta_e \cdot \Delta T/T$, where $\Delta T/T$ is the anisotropy of the radiation at the scattering point. Thus, the isotropic monopole fraction of the radiation is responsible for the classical thermal effect, while the anisotropy of the radiation creates an additional anisotropic effect of a different spectral shape.

For an observer located in nearby clusters, the anisotropy map of the CMB should be nearly identical to that observed at our location including the same $\Delta T/T$ multipoles in both amplitude and orientation with $\ell = 1, 2, 3$. Thus, observation of the CMB radiation scattered by nearby clusters with distorted frequency spectrum gives us a unique opportunity of an independent measurement of the CMB dipole, quadrupole, and octupole.

As for distant clusters, according to Refs. [16,17], observing such a distortion of the spectrum on a large number of clusters is a way to separate the Sachs-Wolfe effect (SW) [22] from the Integrated Sachs-Wolfe effect (ISW) [23] and to some extent get rid of the cosmic variance for multipoles with $\ell = 1, 2, 3$. This is explained by the fact that the integrated effect is formed at very low redshifts and, thus, the spectral distortions caused by the anisotropic SZ effect from high redshift SZ clusters are ISW free.

In our article, we evaluate the practical possibility of detecting an aSZ signal in a real experiment. In this case, the multicomponent nature of the observed signal must be considered, accounting for both relativistic corrections to the SZ effect and foreground signals of various origins.

Since the 1990s, numerous studies have been published addressing various corrections to the Kompaneets equation [24] and SZ effect. Several relativistic corrections to the thermal SZ effect and multiple scattering on SZ clusters are considered in Refs. [25–33]. A study of corrections for the kinematic SZ effect is carried out in Refs. [34–36]. An analytical investigation of the Boltzmann equations was made and expressions for the photon redistribution functions are obtained in Refs. [37–39]. The additional correction to the SZ signal due to the motion of the Solar System is discussed in Ref. [40]. The influence of the CMB anisotropy on the spectral distortions is investigated in Refs. [41–44].

These studies demonstrate that detecting the aSZ is complicated because it must be disentangled from other Sunyaev-Zel'dovich-related spectral distortions. Moreover, foreground signals, including Galactic dust emission, the cosmic infrared background (CIB), synchrotron radiation, free-free emission, and potentially other sources, exceed the target signal by several orders of magnitude, significantly complicating observations and data analysis.

We consider a Fourier transform spectrometer as a target instrument in our modeling. Instruments of this kind have been proven to be suitable for the study of CMB spectral distortions [45,46]. To minimize foregrounds, the instrument should be placed in space [47–49].

Given the experiment's limited sensitivity, a careful approach to data processing is especially important. Not only can this approach facilitate detection of the aSZ signal, but it can also enable separation of other components, revealing the diverse effects arising during the interaction of the CMB with the hot plasma of galaxy clusters. In addition, employing optimal data processing methods for PIXIE-like experiments [48,50] enhances the detectability of μ distortions [51–56] originating in the prerecombination epoch.

The data processing approach must account for our poor knowledge of the expected spectra of some components (for example, dust emission) whose parameters vary unpredictably along the line of sight.

In Refs. [57,58], the Least Response Method (LRM) algorithm is developed for separating signals of interest from photon noise and foreground components with poorly defined spectra. Other known methods such as Internal Linear Combination (ILC) [59] and its modifications: constrained ILC (cILC) and moment ILC (mILC) [60–64] have proven to be insufficiently effective for our analysis. They either fail to remove foregrounds (ILC), or, having removed them all (mILC), fail to sufficiently suppress the contribution of photon noise. LRM minimizes the response to all foregrounds and noise simultaneously, leaving the response to the signal of interest constant. Unlike cILC or mILC, LRM does not require complete orthogonalization of the signal of interest to all other components; that is, the linear filtering of the observed signal across frequency channels does not completely cancel out the contribution from these components. This property mitigates the impact of photon noise. As a result, the desired signal can be detected with lower experimental sensitivity.

In our paper, we apply the LRM for finding the aSZ signal in simulated data. The aim of this approach is to roughly estimate the required experimental sensitivity for aSZ observations and to test the mentioned multifrequency data processing method. In this initial analysis, we do not take into account the kinematic SZ effect and its relativistic corrections.

The paper is organized as follows. In Sec. II, we review the anisotropic Sunyaev-Zel'dovich effect and describe foreground models. In Sec. III, we review the LRM method. In Sec. IV, we present our numerical results. Finally, in Sec. V, we provide our brief conclusions.

II. ANISOTROPIC THERMAL SZ EFFECT AND FOREGROUNDS

In this section, we characterize 1) the spectral distortion generated by anisotropic radiation scattering off galaxy clusters as our signal of interest and 2) the primary foreground components that challenge its detection.

A. ASZ

To describe the anisotropic SZ effect, we use the usual notations. $I = I(\nu)$ is the spectral radiance, which is related to the photon number density as $n(\nu) = \frac{c^2 I}{2h\nu^3}$, where ν, c, h are the frequency, the speed of light, and the Planck constant, respectively. T_e is the temperature of electrons, T_r is the mean temperature of radiation, m_e is the rest mass of the electron, N_e is the concentration of electrons, σ_T is the Thomson cross section, and $\Theta_e = \frac{k_B T_e}{m_e c^2}$, where k_B is the Boltzmann constant.

We consider the scattering of anisotropic radiation on a stationary cloud of hot electrons located within a galaxy cluster. The frequency spectrum of the radiation before scattering $n_0(\nu)$ has a blackbody shape:

$$n_0(x) = B(x) = \frac{1}{e^x - 1}, \quad x = \frac{h\nu}{k_B T_r}. \tag{1}$$

We choose a local spherical coordinate system $\mathbf{\Omega}(\theta, \varphi)$ with the center at the scattering point and the north pole pointing to the observer. In this coordinate system, the temperature of the radiation $T(\mathbf{\Omega})$ incident on the cluster can be decomposed into spherical harmonics $Y_{\ell m}$:

$$\frac{T(\mathbf{\Omega})-T_r}{T_r}=\sum_{\ell m}\tilde{a}_{\ell m}\tilde{Y}_{\ell m}(\mathbf{\Omega}). \tag{2}$$

Note that $\tilde{a}_{\ell m}, \tilde{Y}_{\ell m}$ are not the same as $a_{\ell m}, Y_{\ell m}$ that belong to the conventional Galactic coordinate system at our location.

In Ref. [16], it is shown that, as a result of scattering in the optically thin limit and for $T_r \ll T_e$, $\Theta_e \ll 1$, the frequency spectrum distortion $\Delta_n = n(x) - n_0(x)$ looks as follows:

$$\begin{aligned}\Delta_n/\tau = (\gamma_1+\Theta_e\gamma_2)\left(-x\frac{dB}{dx}\right) + & \quad \Big\}1\\ +\Theta_e\gamma_3\frac{1}{x^2}\frac{d}{dx}\left[x^4\frac{d}{dx}\left(-x\frac{dB}{dx}\right)\right] + & \Big\}2\ (aSZ)\\ +\Theta_e\frac{1}{x^2}\frac{d}{dx}\left[x^4\frac{dB}{dx}\right], & \quad \Big\}3\ (tSZ)\\ \tau = \int N_e\sigma_T dr. &\end{aligned} \tag{3}$$

The third term in Eq. (3) represents the classical tSZ for the isotropic fraction of radiation with the temperature $T_r = \frac{1}{4\pi}\int T(\mathbf{\Omega})d\mathbf{\Omega}$, which corresponds to the monopole $\ell = 0$ in Eq. (2), while the first two terms are due to the presence of CMB anisotropy. According to Ref. [16] only multipoles with $\ell = 1, 2, 3$ distort the signal. The coefficients $\gamma_1, \gamma_2, \gamma_3$ depend on the magnitude and orientation of the CMB dipole, quadrupole, and octupole at the position of scattering,

$$\begin{aligned}\gamma_1 &= \frac{1}{4\sqrt{\pi}}\left(\frac{1}{\sqrt{5}}\tilde{a}_{20} - 2\frac{\Delta_T(\mathbf{\Omega}_z)}{T_r}\right),\\ \gamma_2 &= -\frac{3}{2\sqrt{\pi}}\left(\frac{2}{5\sqrt{3}}\tilde{a}_{10}+\frac{1}{\sqrt{5}}\tilde{a}_{20}-\frac{2}{5\sqrt{7}}\tilde{a}_{30}\right),\\ \gamma_3 &= -\frac{3}{4\sqrt{\pi}}\left(\frac{4}{5\sqrt{3}}\tilde{a}_{10}-\frac{1}{3\sqrt{5}}\tilde{a}_{20}+\frac{1}{5\sqrt{7}}\tilde{a}_{30}\right),\end{aligned} \tag{4}$$

where $\mathbf{\Omega}_z$ is the direction along the z axis to the observer (to the north pole) and $\Delta_T(\mathbf{\Omega}) = T(\mathbf{\Omega}) - T_r$. It should be noted that the spectral distortions are produced only by the anisotropy of the incident radiation that is symmetrical relative to the z axis, i.e., by components with $m = 0$.

The deviation of the form $-x\frac{dB}{dx}$ [the first term in Eq. (3)] is of no interest to us since its shape coincides with the spectral variations caused by the observed temperature anisotropy. Indeed, $\frac{dB}{dT} = -\frac{x}{T}\frac{dB}{dx}$. At the same time, the distortion $\sim\frac{1}{x^2}\frac{d}{dx}[x^4\frac{d}{dx}(-x\frac{dB}{dx})]$ [the second term in Eq. (3)] has a very characteristic spectral form, which allows us to separate it from other components of the observed signal. For convenience, in Ref. [16], this distortion is called the aSZ. It is important to note that, according to Eq. (3), the amplitudes of the anisotropic and thermal effects are both proportional to $\tau\Theta_e$. That is, the ratio of these amplitudes does not depend on the properties of the medium of the observed galaxy cluster. This makes it possible to directly estimate the coefficient γ_3 when both effects are observed simultaneously. Thus, the component of the spectrum observed from a cluster of galaxies in the form of the aSZ is considered as the signal of interest:

$$\begin{aligned}I_{\mathrm{asz}}(\nu) &= A_{\mathrm{asz}}x\frac{d}{dx}\left[x^4\frac{d}{dx}\left(-x\frac{dB}{dx}\right)\right],\\ A_{\mathrm{asz}} &= \frac{2(k_BT_r)^3}{(hc)^2}\tau\Theta_e\gamma_3\end{aligned} \tag{5}$$

Here, the values toward a rich cluster of galaxies are as follows: $\tau \approx 1/100$, $\Theta_e = 7.5\ \mathrm{keV}/511\ \mathrm{keV}$, and $\gamma_3 \sim 5\cdot 10^{-6}$. Hence, $A_{\mathrm{asz}} \approx 0.2\ \mathrm{Jy/sr}$.

Considering the fact that the dipole, quadrupole, and octupole contribute to the amplitude of the same frequency distortion, separating these contributions is only possible by measuring the spectrum from several clusters close to us, i.e., from clusters where these multipoles have the same fixed orientations and $\Delta T/T$ amplitudes as at our location. In total, it is necessary to measure such a distortion from at least 15 clusters in order to separate the contributions from $a_{\ell m}$, $\ell = 1, 2, 3$, $-\ell \le m \le \ell$ (from three dipole components, five quadrupole components, and seven octupole components). Using the expression for γ_3 in Eq. (4), and also taking into account that $a_{\ell m} \sim 1/\sqrt{\ell(\ell+1)}$ for low multipoles, one can estimate the magnitudes of the contributions from $\ell = 1, 2, 3$ anisotropy to the overall effect:

$$\begin{aligned}A_{\mathrm{asz}} &= A_{\mathrm{asz}}^{\ell=1} + A_{\mathrm{asz}}^{\ell=2} + A_{\mathrm{asz}}^{\ell=3},\\ &A_{\mathrm{asz}}^{\ell=2}/A_{\mathrm{asz}}^{\ell=1} \sim 0.19, \qquad A_{\mathrm{asz}}^{\ell=3}/A_{\mathrm{asz}}^{\ell=1} \sim 0.07.\end{aligned} \tag{6}$$

Therefore, the dipole component of the temperature anisotropy dominates this effect. Detecting the contribution from the octupole component requires significantly greater experimental sensitivity.

B. Foregrounds

In our approach, foregrounds are divided by their nature into two types: foregrounds with well-defined spectral shapes and foregrounds with poorly defined spectra. Poorly defined spectra are parametrized spectra with floating parameters. However, these parameters can change only within a limited range of their possible variations. In addition, the amplitudes of all foregrounds cannot exceed certain preestimated values. Foregrounds with poorly defined spectra include dust emission, the CIB, and synchrotron radiation.

Dust and CIB are considered together and modeled as a modified blackbody radiation with two floating parameters,

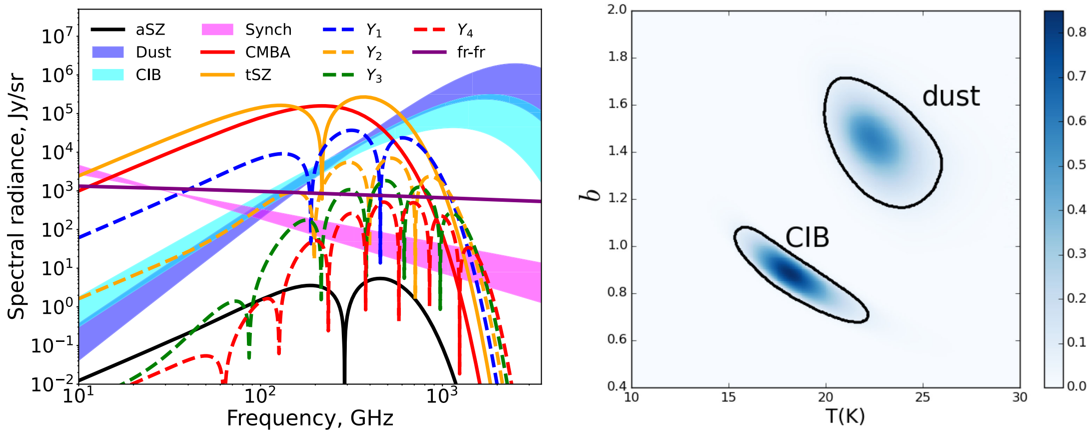

FIG. 1. *Left panel*: spectra of the aSZ signal and main foregrounds. Emissions from dust, the CIB, and the synchrotron are poorly defined spectra with floating parameters. Shaded areas show possible variations of these spectra. The remaining spectra have strictly defined and well-known shapes: CMB anisotropy, thermal SZ effect, the first four relativistic corrections to it Y_1, Y_2, Y_3, Y_4, and the spectrum of free-free transitions. *Right panel*: probability distribution function of the T and b parameters for dust and CIB at Galactic latitudes greater than 30° or less than −30°. The thermal dust is extracted from the Planck Data Release 3 (PDR3) "Commander" maps. The CIB parameters are constructed from PDR2 GNILC maps for CIB at 353, 545, and 857 GHz by fitting a three-parameter modified blackbody.

temperature T and spectral index b,

$$I_{\rm dust}(\nu,T_d,b_d)=A_d(\nu/\nu_0)^{b_d}x_d^3B(x_d),\qquad x_d=\frac{h\nu}{k_BT_d},$$
$$I_{\rm CIB}(\nu,T_c,b_c)=A_c(\nu/\nu_0)^{b_c}x_c^3B(x_c),\qquad x_c=\frac{h\nu}{k_BT_c},\qquad (7)$$

where $\nu_0=353$ GHz. The ranges of possible variations of T_d, b_d and T_c, b_c are shown in Fig. 1 (right panel) for relatively clean parts of the sky. The maximum allowable values for both A_d and A_c are estimated as $3\cdot 10^6$ Jy/sr.

Synchrotron radiation is modeled according to Refs. [65,66], and its spectrum is

$$I_{\rm sync}(\nu,b_s)=A_s(\nu/\nu_s)^{-b_s},\qquad (8)$$

where b_s is the only free parameter with possible variations $0.9\le b_s\le 1.4$. Here, $\nu_s=30$ GHz, and $A_s\approx 1000$ Jy/sr. The values of A_s and b_s were extracted from QUIJOTE [66] sky maps at Galactic latitudes greater than 30° or less than −30°.

For foregrounds with well-defined spectra, we consider free-free emission and corrections associated with modifications of the blackbody spectrum of the relic radiation.

Free-free emission is given by the formula [67]

$$I_{ff}(\nu)=A_{ff}\left(1+\ln\left[1+\left(\frac{\nu_{ff}}{\nu}\right)^{\sqrt{3}/\pi}\right]\right),$$
$$\nu_{ff}=255.33\ {\rm GHz}(T/10^3\ {\rm K})^{3/2},\qquad (9)$$

where $A_{ff}=300$ Jy/sr and T is the electron temperature. According to component maps provided by the Planck Collaboration [67], T is distributed between 6995 and 7030 K with a sharp peak at 7000 K. Consequently, we assume $\nu_{ff}\approx 4728$ GHz and this parameter does not vary much across the sky to noticeably change the shape of the spectrum. Thus, in our calculations, we consider the free-free spectrum as a well-defined one.

Other foregrounds with well-defined spectra include the CMB temperature anisotropy, which is the first derivative of $B(x)$ with respect to radiation temperature T_r, and four relativistic corrections to the thermal SZ effect,

$$I_{\rm CMBA}(\nu)=A_{\rm CMBA}x^4\frac{dB}{dx},$$
$$I_{y_0}(\nu)=A_{y_0}x\frac{d}{dx}\left[x^4\frac{dB}{dx}\right],$$
$$I_{y_n}(\nu)=A_{y_n}\frac{x^4e^x}{(e^x-1)^2}Y_n(x),\qquad n=1,\ldots,4,$$
$$A_{y_0}=\frac{2(k_BT_r)^3}{(hc)^2}\tau\Theta_e,\qquad A_{y_n}=A_{y_0}\Theta_e^n,\qquad (10)$$

where $x=h\nu/k_BT_r$, $T_r=2.72548\ K$ [68,69], $A_{\rm CMBA}\le 3.24\cdot 10^4$ Jy/sr, and $A_{y_0}\approx 4\cdot 10^4$ Jy/sr.

The functions $Y_n(x)$, $n\ge 1$ for the relativistic corrections have a rather cumbersome form, and analytical formulas for them can be found in Ref. [28].

Another additional term in the observed signal is photon noise, which appears in each frequency channel as a random value. It comes from the CMB radiation, a number of main foregrounds, and emission from the instrument including the optical system of the telescope. The magnitude of noise and its possible correlations between different frequency channels can be estimated in the process of observing the same galaxy cluster by subtracting from each other the signals observed at different times over the same time intervals.

The spectra of the foregrounds and the aSZ signal are presented in Fig. 1 (left panel).

III. COMPONENT SEPARATION USING THE LEAST RESPONSE METHOD

The Least Response Method is a linear filtering of the observed signal that minimizes the response to all foregrounds and noise while keeping the response to the desired signal constant. It has the following distinctive features:

(1) It does not require complete orthogonalization of the various signal components. In other words, when determining the contribution of any component, this method does not completely cancel out the contributions of the remaining components with known spectra. This significantly reduces the impact of photon noise on the recovered component amplitudes. For example, if we have two components, one of which is significantly larger than the other, when finding the larger component, the LRM practically ignores the smaller one, instead of setting it to zero and thereby increasing the response to white noise.

(2) It assumes our knowledge of the limits of possible variation of the foreground spectral parameters for those foregrounds whose spectra are poorly defined.

As shown in the previous section, the observed frequency spectrum $S(\nu)$ can be divided into two parts,

$$S(\nu) = I(\nu) + \tilde{I}(\nu), \tag{11}$$

where $I(\nu)$ consists of components with well-defined spectral shapes, while $\tilde{I}(\nu)$ includes components with poorly defined spectra. In general, one can consider a total signal consisting of M components of different physical origin with well-defined spectra and K components with poorly defined spectra:

$$I(\nu) = \sum_{m=1}^{M} I^m(\nu), \qquad \tilde{I}(\nu) = \sum_{k=1}^{K} \tilde{I}^k(\nu). \tag{12}$$

Each component $I^m(\nu)$ with a fixed spectral shape is described either by a known analytical function or by a strictly defined template $f^m(\nu)$,

$$I^m(\nu) = \alpha_m f^m(\nu), \quad m = 1, \ldots, M, \tag{13}$$

where α_m is the amplitude of the mth component. Such components in the observed signal may include, for example, the thermal SZ effect, relativistic corrections to it, or the anisotropic SZ effect.

When processing observational data using the LRM method, it is assumed that the amplitudes α_m cannot exceed certain preestimated limits:

$$|\alpha_m| \leq A_m \quad m = 1, \ldots, M. \tag{14}$$

Such upper limits on the amplitudes of various effects can be found from previous observations and numerical estimates.

As for components with poorly defined spectra, they can usually also be described by analytical functions $\tilde{f}^k(\nu, \boldsymbol{P_k})$, $k = 1, \ldots, K$. Unlike well-defined components, the shapes of their spectra depend on the set of parameters $\boldsymbol{P_k}$ and change when these parameters are varied. One example of such a component is the emission of thermal dust. The uncertainty in the spectra arises from the integration of the signal along the line of sight, where the radiation from dust changes its parameters, such as temperature or the slope of the spectrum.

Similar to Eq. (13), the observed spectrum from such components can be written as

$$\begin{aligned} \tilde{I}^k(\nu) &= \frac{1}{V_{\tilde{\Omega}_k}} \int_{\tilde{\Omega}_k} \tilde{\alpha}_k(\mathbf{P_k}) \tilde{f}^k(\nu, \mathbf{P_k}) d\mathbf{P_k}, \\ d\mathbf{P_k} &= dp_1^k dp_2^k \cdot \cdot dp_{L_k}^k, \quad k = 1, \ldots, K, \\ V_{\tilde{\Omega}_k} &= \int_{\tilde{\Omega}_k} d\mathbf{P_k}, \end{aligned} \tag{15}$$

where $\mathbf{P_k} = p_1^k, \ldots, p_{L_k}^k$ is the set of L_k parameters of the kth component and $\tilde{\Omega}_k$ is the range of possible variations of these parameters. $\tilde{\Omega}_k$ for each of the poorly defined components can be determined from the results of the previous experiments such as Planck and WMAP. Analogously to Eq. (14), we also assume that the amplitudes of the spectra $\tilde{\alpha}_k$ are less than some preestimated values,

$$|\tilde{\alpha}_k(\mathbf{P_k})| \leq \tilde{A}_k \quad \text{for } \mathbf{P_k} \in \tilde{\Omega}_k, \tag{16}$$

and $\tilde{\alpha}_k(\mathbf{P_k}) = 0$ otherwise. Therefore, we do not know the exact shapes of the frequency spectra $\tilde{I}_k$ that contribute to the overall observed spectrum but only know the limitations determined by Eqs. (15) and (16) on the signal they create.

During the observations in each sky pixel, we will observe a discrete signal S_j in J frequency channels ν_j, consisting of the terms

$$S_j = \sum_{m=1}^{M} \alpha_m f_j^m + \sum_{k=1}^{K} \tilde{I}_j^k + N_j, \quad j = 1, \ldots, J, \tag{17}$$

where $f_j^m = f^m(\nu_j)$, $\tilde{I}_j^k = \tilde{I}^k(\nu_j)$ and N_j is the photon noise. For convenience, this equation can be written in vector form,

$$\mathbf{S} = \mathbf{F} + \tilde{\mathbf{F}} + \mathbf{N}, \quad \mathbf{F} = \sum_{m=1}^{M} \alpha_m \mathbf{f^m}, \qquad \tilde{\mathbf{F}} = \sum_{k=1}^{K} \tilde{\mathbf{I}}^{\mathbf{k}}, \quad (18)$$

where bold symbols $\mathbf{X}$ denote row vectors $\boldsymbol{X} = (X_1 \cdots X_J)$. Here, $\boldsymbol{F}$ is the sum of components with well-defined spectra, $\tilde{\boldsymbol{F}}$ contains all foregrounds with poorly defined spectra, and $\boldsymbol{N}$ is the noise with zero mean and covariance matrix $[C_{ij}] = \mathbf{C} = \langle \mathbf{N^T N} \rangle$.

Our task is to estimate with the best accuracy all the coefficients α_m for components with well-defined spectral shapes, leaving untouched the poorly defined part of the observed spectrum. That is, we need to find the vector $\boldsymbol{\alpha} = (\alpha_1 \cdots \alpha_M)$. For each component number m, the LRM method finds the optimal row vector of weights $\boldsymbol{\omega^m} = (\omega_1^m \cdots \omega_J^m)$. This vector ensures for linear filtering the unit response to this component: $\boldsymbol{\omega^m f^{mT}} = 1$ and a minimal response to all other components and photon noise. Thus, we can introduce a matrix of the size $J \times M$ whose columns are represented by the components of the row vectors $\boldsymbol{\omega^m}$:

$$\mathbf{W} = \begin{pmatrix} \boldsymbol{\omega}^{1T} & \boldsymbol{\omega}^{2T} & \cdot & \cdot & \boldsymbol{\omega}^{MT} \end{pmatrix} = \begin{pmatrix} \omega_1^1 & \omega_1^2 & . & . & \omega_1^M \\ \omega_2^1 & \omega_2^2 & . & . & \omega_2^M \\ . & . & . & . & . \\ \omega_J^1 & \omega_J^2 & . & . & \omega_J^M \end{pmatrix}. \quad (19)$$

By multiplying the observed signal vector $\mathbf{S}$ by the matrix $\mathbf{W}$, we obtain an estimate for the amplitude vector $\boldsymbol{\alpha}$,

$$\bar{\boldsymbol{\alpha}} = \mathbf{SW} = \boldsymbol{\alpha} + \boldsymbol{R}, \quad (20)$$

where the components R_m of the vector $\mathbf{R}$ are

$$R_m = \left[\sum_{m' \neq m} \alpha_{m'} \mathbf{f^{m'}} + \tilde{\mathbf{F}} + \mathbf{N} \right] \boldsymbol{\omega^{mT}}, \quad m = 1, \ldots, M, \quad (21)$$

and the summation is performed over all m' from 1 to M except $m' = m$. In Ref. [58], it is shown that the best weights for each mth component that minimize the response R_m are

$$\boldsymbol{\omega^m} = f^{\mathbf{m}} \mathbf{D}^{-1} \cdot (\mathbf{f^m} \mathbf{D}^{-1} (\mathbf{f^m})^{\mathrm{T}})^{-1}, \qquad \mathbf{D} = \boldsymbol{\Phi}^{\mathbf{m}} + \tilde{\boldsymbol{\Phi}} + \mathbf{C}. \quad (22)$$

Here, $\boldsymbol{\Phi}^m = [\Phi_{ij}^m]$ and $\tilde{\Phi} = [\tilde{\Phi}_{ij}]$ are the $J \times J$ covariance matrices of the foregrounds with well-defined and poorly defined spectra, respectively. They are calculated as follows:

$$\Phi_{ij}^m = \sum_{m' \neq m} A_{m'}^2 q_{ij}^{m'}, \qquad q_{ij}^{m'} = f_i^{m'} f_j^{m'},$$
$$\tilde{\Phi}_{ij} = \sum_{k=1}^{K} \tilde{A}_k^2 \tilde{q}_{ij}^k,$$
$$\tilde{q}_{ij}^k = \frac{1}{V_{\tilde{\Omega}_k}} \cdot \int_{\tilde{\Omega}_k} \tilde{f}_i^k(\mathbf{P_k}) \tilde{f}_j^k(\mathbf{P_k}) d\mathbf{P_k}. \quad (23)$$

As can be seen from Eqs. (20) and (21), for each component m, the difference between its estimated amplitude $\bar{\alpha}_m$ and its true value α_m is determined by the response R_m. This response consists of the response to foregrounds R_m^{fgr} (which are considered to be all other components with $m' \neq m$) and the response to photon noise R_m^{Noise}:

$$\bar{\alpha}_m - \alpha_m = R_m = R_m^{\mathrm{fgr}} + R_m^{\mathrm{Noise}}, \quad m = 1, \ldots, M,$$
$$R_m^{\mathrm{fgr}} = \left[\sum_{m' \neq m} \alpha_{m'} \mathbf{f^{m'}} + \tilde{\mathbf{F}} \right] \boldsymbol{\omega^{mT}},$$
$$R_m^{\mathrm{Noise}} = \mathbf{N} \boldsymbol{\omega^{mT}}. \quad (24)$$

In approaches such as cILC and mILC, the weights $\boldsymbol{\omega^m}$ are calculated with the strict condition of zeroing out the contributions from all foregrounds selected for exclusion from the signal: $R_m^{\mathrm{fgr}} = 0$. This leads to an extremely uneven distribution of the weights ω_j^m and their large values. This significantly increases the response to photon noise R_m^{Noise}. LRM, on the other hand, optimally distributes the response to foregrounds and noise in such a way that their combined response is minimized.

The approach described above not only estimates the amplitudes of signal components better than cILC but also has the potential for improvement. To find the amplitudes α_m, we have safely used the upper possible estimate for all other amplitudes $\alpha_{m'}$, $m' \neq m$. Refining the values α_m can in principle improve the result.

IV. NUMERICAL RESULTS

For the numerical analysis, we use simulations of the signal passing along a single line of sight directed at a galaxy cluster with a plasma temperature of 7.5 keV. The signal in a single pixel consists of discrete values S_j, $j = 1, \ldots, J$ in $J = 384$ frequency channels ν_j covering the range from 10 GHz to 2.9 THz with a channel width of $\Delta\nu = 7.5$ GHz.

We assume that the angular resolution of the experiment, at least for nearby clusters and relatively high-frequency bands $\gtrsim$300 GHz, is high enough for the signal source to be continuous. Galaxy clusters contain most of their SZ signal in the brightest central ∼200 kpc part. This scale has apparent size larger than ∼20 arcsec at any redshift due to the cosmological expansion. With larger beam size, the instrument can collect more foregrounds while collecting

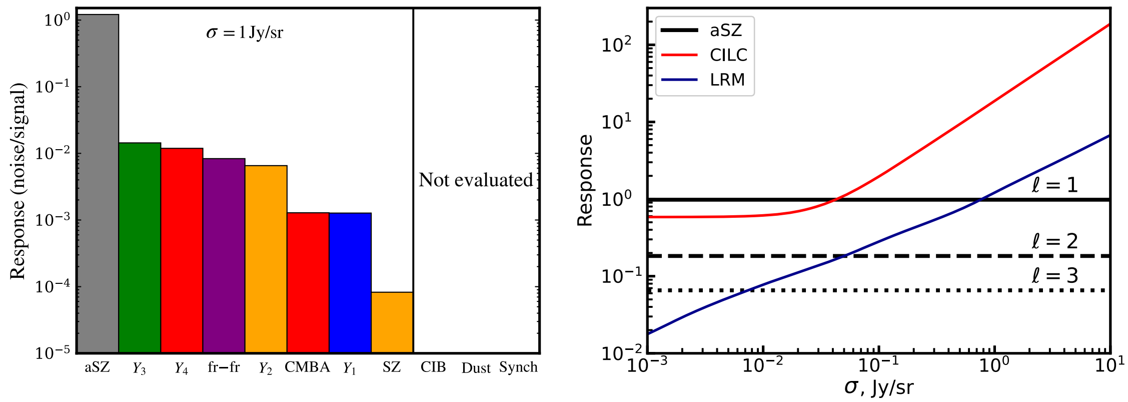

FIG. 2. Application of the LRM method for signal component separation and extraction of the aSZ from the observed spectrum: *Left panel*: the histogram shows the total response to foregrounds and photon noise when extracting a signal with a well-defined spectral shape. The response is equivalent to the noise-to-signal ratio. Foregrounds with poorly defined spectral shapes were not extracted from the observed spectrum. The results were obtained for a sensitivity of 1 Jy/sr per frequency channel using the LRM method. *Right panel*: the red line shows the total response to all foregrounds and noise when extracting the aSZ signal using the cILC approach. The blue line corresponds to the same when using the LRM method. The black horizontal lines correspond to the aSZ signal caused by the dipole ($\ell = 1$), quadrupole ($\ell = 2$), and octupole ($\ell = 3$) components of the CMB anisotropy at the location of the galaxy cluster. The intersection points with the horizontal lines correspond to a signal-to-noise ratio of 1.

almost the same amount of signal, and this will decrease the signal to noise ratio. Smaller beams are technically more challenging, since they require larger apertures. For a cluster at 300 Mpc, the central 200 kpc has angular size of 2 arc min. A space observatory such as Ref. [47] with a primary mirror size of 10 m has a diffraction limit of $\sim$1 arc min at 100 GHz. Therefore, below, we give the required sensitivity in the units of Jy/sr assuming the source is resolved. This can be converted into Jy by assuming a pixel size equal to the apparent size of a central part of a cluster, i.e., 20 arc sec for a distant cluster and $\sim$2 arc min for a nearby cluster.

In accordance with the definitions and descriptions of foregrounds in Secs. II and III, we consider eight components whose spectral shapes are well defined ($M = 8$), three components with poorly defined spectra ($K = 3$), and photon noise. The list of components is as follows:

(1) The *well-defined spectra* [$f^m(\nu_j)$] are:
   (a) $m = 1$: anisotropic SZ effect;
   (b) $m = 2$: thermal SZ effect;
   (c) $m = 3, 4, 5, 6$: first four relativistic corrections to the thermal SZ effect, respectively;
   (d) $m = 7$: spectrum of free-free transitions; and
   (e) $m = 8$: spectrum of the CMB anisotropy.

Here, we do not take into account the spectrum of the CMB monopole, since it can be easily removed from the observational data.

(2) The *poorly defined spectra* ($\tilde{f}^k(\nu_j, \mathbf{P_k})$) are:
   (a) $k = 1$: dust emission with two free parameters $\boldsymbol{P_1} = (T_d, b_d)$, $\boldsymbol{P_1} \in \tilde{\Omega}_1$ [see Eq. (7)];
   (b) $k = 2$: CIB with two free parameters $\boldsymbol{P_2} = (T_c, b_c)$, $\boldsymbol{P_2} \in \tilde{\Omega}_2$ [see Eq. (7)]; and
   (c) $k = 3$: synchrotron radiation with one free parameter $\boldsymbol{P_3} = b_s$, $\boldsymbol{P_3} \in \tilde{\Omega}_3$ [see Eq. (8)].

Here, the possible ranges of parameters variation $\tilde{\Omega}_1, \tilde{\Omega}_2, \tilde{\Omega}_3$ are defined in Sec. II (see also Fig. 1).

(3) We model *photon noise* as white noise with a diagonal covariance matrix $\mathbf{C} = \langle \mathbf{N}^\mathbf{T} \mathbf{N} \rangle$: $C_{ij} = \delta_i^j \sigma^2$. Here, σ is the noise level per single channel. This value can be considered as the sensitivity of the experiment.

In Fig. 2, we demonstrate the results of our numerical experiment using the LRM method, previously tested in Ref. [58], for signal component separation. We do not try to determine the contributions to the overall signal from poorly defined components, i.e., from the CIB, dust, and synchrotron, owing to the lack of information about these spectra.

The left panel shows the result of estimating the signal component amplitudes α_m in the case when the photon noise is 1 Jy/sr in each of the 384 channels. At this sensitivity, all considered components with well-defined spectral shapes are recovered with good accuracy. The only exception is the aSZ, for which the signal-to-noise ratio in this case is $\sim$1.

The right panel shows the results of applying the LRM method to extract the aSZ signal depending on sensitivity, i.e., on σ. We are interested in the sensitivity needed to find the signal of interest, i.e., in this case the anisotropic SZ effect ($m = 1$). The weights $\boldsymbol{\omega}^\mathbf{1}$ are always normalized in such a way that the response to the dipole part of the aSZ is equal to 1. This means that the total response to all other signal components, including noise, can be interpreted as the noise-to-signal ratio. For comparison, we also present the results of applying the cILC method, analogously to how it is done in Ref. [58], where the extraction of the μ distortion from the observed spectrum is considered. This approach gives a result that is approximately 1 order of magnitude worse. Furthermore, similar to the results demonstrated in Ref. [58], as the photon noise becomes less than $\sim$0.02 Jy/sr, the cILC method reaches an asymptotic constant and ceases to improve the result. This occurs due to an insufficiency of derivatives with respect to parameters for foregrounds with poorly defined spectra, which leads to an irreducible response to these components. An increase in the number of derivatives with respect to parameters slightly improves the result for small photon noise and significantly degrades it if the photon noise is large.

Thus, when processing data using the LRM approach, a sensitivity of 1 Jy/sr is sufficient for the response to the aSZ signal, caused by the dipole anisotropy component, to be equal to the response to foregrounds and noise. For the quadrupole anisotropy, this is achieved with a sensitivity of $\sim$0.05 Jy/sr and for the octupole, with $\sigma \sim 0.01$ Jy/sr.

V. CONCLUSIONS

In our paper, we assessed the practical prospects for independent measurement of the CMB anisotropy multipoles with $\ell = 1$, 2, 3 using the anisotropic Sunyaev-Zel'dovich effect.

The LRM method can be effectively applied to any observational data containing components with poorly defined spectra. Beyond studies of the aSZ, one of the most promising applications of this approach is the detection of μ spectral distortions in the CMB.

We have not yet taken into account the kinematic SZ effect. Consequently, our estimate of the sensitivity required for aSZ detection ($\sim$0.05, 0.1 Jy/sr) should be regarded as preliminary and will require further refinement. Adding the kinematic SZ effect and its relativistic corrections will increase the number of components that need to be separated from each other. However, it not only enables detection of CMB anisotropy at the scattering point but also provides critical constraints on 1) the cluster plasma temperature, 2) the cluster's peculiar velocity relative to the CMB rest frame, and 3) its line-of-sight velocity component.

It is important to note that linear polarization occurs as a result of scattering of anisotropic radiation by clusters. The polarization produced as a result of "cold" Thomson scattering in the nonrelativistic regime is considered in Ref. [70] for clusters at high redshifts to measure the CMB quadrupole, thereby getting around cosmic variance. Nevertheless, the relic radiation itself is also initially polarized starting from the recombination epoch. Thus, without considering spectral distortions, it is quite difficult to distinguish between the polarization resulting from scattering on the SZ cluster and the initial CMB polarization. In Ref. [17], it is shown that as a result of the aSZ, in addition to the distortion of the spectral radiance $I(\nu)$, a spectral distortion of the Stokes parameters $Q(\nu)$ and $U(\nu)$ arises as well. Unlike the spectral radiance, the spectrum of the Stokes parameters is distorted only by the quadrupole and octupole of the anisotropy. The dipole and, what is especially important, the CMB monopole do not introduce additional terms. This means that the relativistic thermal corrections from the dominant monopole do not contribute to the distortions of the polarization spectrum and the task of component separation is significantly simplified.

Future work should incorporate the kinematic Sunyaev-Zel'dovich effect, and it would be highly desirable to exploit the linear polarization of radiation from galaxy clusters.

ACKNOWLEDGMENTS

We wish to thank the referee for valuable comments and productive discussion.

DATA AVAILABILITY

There are no publicly available research data or software supporting this manuscript. Requests for further information or data should be sent to the authors.

[1] C. L. Bennett, D. Larson, J. L. Weiland, N. Jarosik, G. Hinshaw, N. Odegard, K. M. Smith, R. S. Hill, B. Gold, M. Halpern *et al.*, Astrophys. J., Suppl. Ser. **208**, 20 (2013).

[2] P. A. R. Ade, N. Aghanim, C. Armitage-Caplan, M. Arnaud, M. Ashdown, F. Atrio-Barandela, J. Aumont, C. Baccigalupi, A. J. Banday *et al.* (Planck Collaboration), Astron. Astrophys. **571**, A15 (2014).

[3] Y. Akrami, M. Ashdown, J. Aumont, C. Baccigalupi, M. Ballardini, A. J. Banday, R. B. Barreiro, N. Bartolo, S. Basak *et al.* (Planck Collaboration), Astron. Astrophys. **641**, A4 (2020).

[4] C. J. Copi, D. Huterer, and G. D. Starkman, Phys. Rev. D **70**, 043515 (2004).

[5] C. J. Copi, D. Huterer, D. J. Schwarz, and G. D. Starkman, Mon. Not. R. Astron. Soc. **367**, 79 (2006).

[6] P. D. Naselsky and O. V. Verkhodanov, Int. J. Mod. Phys. D **17**, 179 (2008).

[7] G. Efstathiou, Mon. Not. R. Astron. Soc. **346**, L26 (2003).

[8] M. Tegmark, A. de Oliveira-Costa, and A. J. Hamilton, Phys. Rev. D **68**, 123523 (2003).
[9] D. J. Schwarz, G. D. Starkman, D. Huterer, and C. J. Copi, Phys. Rev. Lett. **93**, 221301 (2004).
[10] C. J. Copi, D. Huterer, D. J. Schwarz, and G. D. Starkman, Adv. Astron. **2010**, 847541 (2010).
[11] S. Nadathur, M. Lavinto, S. Hotchkiss, and S. Räsänen, Phys. Rev. D **90**, 103510 (2014).
[12] Y. Wang and Y.-Z. Ma, Nucl. Phys. **B906**, 367 (2016).
[13] P. A. R. Ade, N. Aghanim, Y. Akrami, P. K. Aluri, M. Arnaud, M. Ashdown, J. Aumont, C. Baccigalupi, A. J. Banday *et al.* (Planck Collaboration), Astron. Astrophys. **594**, A16 (2016).
[14] D. J. Schwarz, C. J. Copi, D. Huterer, and G. D. Starkman, Classical Quantum Gravity **33**, 184001 (2016).
[15] J. Creswell and P. Naselsky, J. Cosmol. Astropart. Phys. 03 (2021) 103.
[16] I. G. Edigaryev, D. I. Novikov, and S. V. Pilipenko, Phys. Rev. D **98**, 123513 (2018).
[17] D. I. Novikov, S. V. Pilipenko, M. De Petris, G. Luzzi, and A. O. Mihalchenko, Phys. Rev. D **101**, 123510 (2020).
[18] J. Chluba, D. Nagai, S. Sazonov, and K. Nelson, Mon. Not. R. Astron. Soc. **426**, 510 (2012).
[19] Y. B. Zeldovich and R. A. Sunyaev, Astrophys. Space. Sci. **4**, 301 (1969).
[20] R. A. Sunyaev and Y. B. Zeldovich, Astrophys. Space. Sci. **7**, 20 (1970).
[21] J. P. Babuel-Peyrissac and G. Rouvillois, J. Phys. (Paris) **30**, 301 (1969).
[22] R. K. Sachs and A. M. Wolfe, Astrophys. J. **147**, 73 (1967).
[23] M. J. Rees and D. W. Sciama, Nature (London) **217**, 511 (1968).
[24] A. S. Kompaneets, Sov. J. Exp. Theor. Phys. **4**, 730 (1957), https://ui.adsabs.harvard.edu/abs/1957JETP....4..730K.
[25] J. Chluba, R. Khatri, and R. A. Sunyaev, Mon. Not. R. Astron. Soc. **425**, 1129 (2012).
[26] J. Chluba, L. Dai, and M. Kamionkowski, Mon. Not. R. Astron. Soc. **437**, 67 (2014).
[27] J. Chluba and L. Dai, Mon. Not. R. Astron. Soc. **438**, 1324 (2014).
[28] A. Challinor and A. Lasenby, Astrophys. J. **499**, 1 (1998).
[29] N. Itoh, Y. Kohyama, and S. Nozawa, Astrophys. J. **502**, 7 (1998).
[30] A. Stebbins, arXiv:astro-ph/9709065.
[31] M. Shimon and Y. Rephaeli, Astrophys. J. **575**, 12 (2002).
[32] N. Itoh, Y. Kawana, S. Nozawa, and Y. Kohyama, Mon. Not. R. Astron. Soc. **327**, 567 (2001).
[33] W. Hu, D. Scott, and J. Silk, Phys. Rev. D **49**, 648 (1994).
[34] S. Nozawa, N. Itoh, and Y. Kohyama, Astrophys. J. **508**, 17 (1998).
[35] S. Y. Sazonov and R. A. Sunyaev, Astrophys. J. **508**, 1 (1998).
[36] A. Challinor and A. Lasenby, Astrophys. J. **510**, 930 (1999).
[37] S. Nozawa and Y. Kohyama, Phys. Rev. D **79**, 083005 (2009).
[38] S. Nozawa and Y. Kohyama, Mon. Not. R. Astron. Soc. **434**, 710 (2013).
[39] S. Nozawa and Y. Kohyama, Mon. Not. R. Astron. Soc. **441**, 3018 (2014).
[40] J. Chluba, G. Hütsi, and R. A. Sunyaev, Astron. Astrophys. **434**, 811 (2005).
[41] S. Yasini and E. Pierpaoli, Phys. Rev. D **94**, 023513 (2016).
[42] S. A. Balashev, E. E. Kholupenko, J. Chluba, A. V. Ivanchik, and D. A. Varshalovich, Astrophys. J. **810**, 131 (2015).
[43] S. Yasini and E. Pierpaoli, Phys. Rev. Lett. **119**, 221102 (2017).
[44] P. d. S. Ferreira and M. Quartin, Phys. Rev. Lett. **127**, 101301 (2021).
[45] D. J. Fixsen, E. S. Cheng, J. M. Gales, J. C. Mather, R. A. Shafer, and E. L. Wright, Astrophys. J. **473**, 576 (1996).
[46] P. de Bernardis, S. Colafrancesco, G. D'Alessandro, L. Lamagna, P. Marchegiani, S. Masi, and A. Schillaci, Astron. Astrophys. **538**, A86 (2012).
[47] I. D. Novikov, S. F. Likhachev, Y. A. Shchekinov, A. S. Andrianov, A. M. Baryshev, A. I. Vasyunin, D. Z. Wiebe, T. d. Graauw, A. G. Doroshkevich, I. I. Zinchenko *et al.*, Phys. Usp. **64**, 386 (2021).
[48] A. Kogut, J. Chluba, D. J. Fixsen, S. Meyer, and D. Spergel, in *Space Telescopes and Instrumentation 2016: Optical, Infrared, and Millimeter Wave*, edited by H. A. MacEwen, G. G. Fazio, M. Lystrup, N. Batalha, N. Siegler, and E. C. Tong, Society of Photo-Optical Instrumentation Engineers (SPIE) Conference Series (SPIE, Bellingham, WA, 2016), Vol. 9904, p. 99040W.
[49] J.-P. Maillard, Phil. Trans. R. Soc. A **379**, 20200212 (2021).
[50] J. C. Hill, N. Battaglia, J. Chluba, S. Ferraro, E. Schaan, and D. N. Spergel, Phys. Rev. Lett. **115**, 261301 (2015).
[51] R. A. Sunyaev and Y. B. Zeldovich, Astrophys. Space Sci. **9**, 368 (1970).
[52] W. Hu and J. Silk, Phys. Rev. Lett. **70**, 2661 (1993).
[53] R. Khatri and R. A. Sunyaev, J. Cosmol. Astropart. Phys. 09 (2012) 016.
[54] J. Chluba, A. L. Erickcek, and I. Ben-Dayan, Astrophys. J. **758**, 76 (2012).
[55] J. Yang, X. Wang, X.-H. Ma, D. Zhang, S.-F. Yan, A. Ilyas, and Y.-F. Cai, Phys. Rev. D **111**, 043522 (2025).
[56] J. Mastache, W. Barrera, and R. Henríquez-Ortiz, J. Cosmol. Astropart. Phys. 05 (2024) 070.
[57] D. I. Novikov and A. O. Mihalchenko, Phys. Rev. D **107**, 063506 (2023).
[58] J. P. Maillard, A. Mihalchenko, D. Novikov, A. Osipova, S. Pilipenko, and J. Silk, Phys. Rev. D **109**, 023523 (2024).
[59] G. B. Rybicki and W. H. Press, Astrophys. J. **398**, 169 (1992).
[60] M. Remazeilles, J. Delabrouille, and J.-F. Cardoso, Mon. Not. R. Astron. Soc. **418**, 467 (2011).
[61] M. Remazeilles and J. Chluba, Mon. Not. R. Astron. Soc. **494**, 5734 (2020).
[62] V. Stolyarov, M. P. Hobson, A. N. Lasenby, and R. B. Barreiro, Mon. Not. R. Astron. Soc. **357**, 145 (2005).
[63] J. Chluba, J. C. Hill, and M. H. Abitbol, Mon. Not. R. Astron. Soc. **472**, 1195 (2017).

[64] A. Rotti and J. Chluba, Mon. Not. R. Astron. Soc. **500**, 976 (2021).

[65] G. B. Rybicki and A. P. Lightman, *Radiative Processes in Astrophysics* (Wiley-VCH, New York, 1986).

[66] E. de la Hoz, R. B. Barreiro, P. Vielva, E. Martínez-González, J. A. Rubiño-Martín, B. Casaponsa, F. Guidi, M. Ashdown, R. T. Génova-Santos, E. Artal *et al.*, Mon. Not. R. Astron. Soc. **519**, 3504 (2023).

[67] R. Adam, P. A. R. Ade, N. Aghanim, M. I. R. Alves, M. Arnaud, M. Ashdown, J. Aumont, C. Baccigalupi, A. J. Banday *et al.* (Planck Collaboration), Astron. Astrophys. **594**, A10 (2016).

[68] J. C. Mather, E. S. Cheng, R. E. Eplee, Jr., R. B. Isaacman, S. S. Meyer, R. A. Shafer, R. Weiss, E. L. Wright, C. L. Bennett, N. W. Boggess *et al.*, Astrophys. J. Lett., **354**, L37 (1990).

[69] D. J. Fixsen, Astrophys. J. **707**, 916 (2009).

[70] M. Kamionkowski and A. Loeb, Phys. Rev. D **56**, 4511 (1997).